An Energy-Autonomous Wireless Sensor with Simultaneous Energy Harvesting and Ambient Light Sensing

Roberto La Rosa, Catherine Dehollain, Andreas Burg, Mario Costanza and Patrizia Livreri

***Abstract*— Wireless sensor nodes (WSNs) are generally powered by batteries, which results in a substantial limitation to the places where the nodes can be installed, to the maximum number of deployable devices, and to the node lifetime. To meet the demand for Internet-of-Things (IoT) applications that require a large number of maintenance-free, low cost, wireless sensor nodes, this paper proposes a wireless sensor platform with a single photovoltaic transducer that performs the dual role of harvesting energy and sensing ambient light. This dual use allows even smaller and cheaper nodes that do not require any form of supporting external power, with a reduced component count. The device implements off-the-shelf components on a 2 x 2 cm^2 printed circuit board (PCB) with a thickness of 0.45 cm. It features Bluetooth Low Energy (BLE) communication and can harvest and sense indoor ambient light with a limit of detection of 200 lux.**

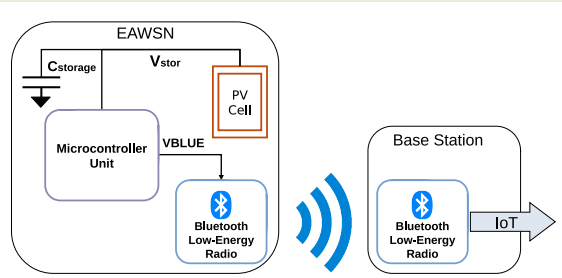

***Index Terms*— Bluetooth Low Energy, Energy harvesting, Internet of Things (IoT), light sensors, low power, Microcontroller, Wireless Sensor Network, Wireless Sensor Node, Home Automation**

I. Introduction

Internet of Things (IoT) solutions using wireless sensor networks are finding increasing application in building automation infrastructure thanks to advanced technologies that assist and improve the quality of life of occupants. They are principally used to ensure stable and comfortable ambient conditions while driving energy savings through continuous monitoring of environmental factors such as humidity, light intensity, noise levels, etc. [1], [2]. This context is a clear promoter of sensor technologies that can deliver increasingly numerous wireless, maintenance free, and inexpensive sensing devices that can be deployed in virtually any location [3], [4]. Wireless sensor nodes are generally battery-powered and are more often than not beset with difficulties associated with power consumption. Engineers are in fact on the perpetual hunt for elusive combinations of size and cost reduction, while still delivering greater range and longer battery life. A current trend in this direction is the adoption of energy-efficient communication technologies such as ZigBee and Bluetooth Low Energy (BLE), which use the license-free industrial and scientific and medical (ISM) band [5], [6]. Nevertheless, the major challenge of how to manage and supply power to the node effectively remains. All this suggests, where possible, to use energy harvesting (EH) and wireless power transfer (WPT) [7]. Earlier publications show various techniques for improving the performance of battery-powered devices. Some involve techniques to eliminate energy consumption during the standby phase [8], while others are centered on achieving energy autonomy by combining EH and rechargeable batteries [9], [10]. Even though these results indeed extend device autonomy, or facilitate miniaturization, or both, they cannot completely resolve the underlying problems. Battery-less devices, on the other hand, circumvent problems associated with batteries, including lifetime limitations, the physical and labor intensive cost of replacement, and their susceptibility to environmental conditions [11]–[16]. The research papers published in this field, however, are mostly conceptual proposals and theoretical studies with only few actual implementations [9]. This paper presents the design and implementation of a novel battery-free BLE ambient light sensor using a single photovoltaic (PV) cell to perform both energy harvesting and sensing [17], [18]. This approach requires less

This paragraph of the first footnote will contain the date on which you submitted your paper for review. It will also contain support information, including sponsor and financial support acknowledgment. For example, "This work was supported in part by the U.S. Department of Commerce under Grant BS123456."

Roberto La Rosa is with STMicroelectronics, 95125 Catania, Italy and also with Ecole Polytechnique Federale de Lausanne, Switzerland (e-mail: roberto.larosa@st.com).

Catherine Dehollain is with Ecole Polytechnique Federale de Lausanne, Switzerland (e-mail: catherine.dehollain@epfl.ch).

Andreas Burg is with Ecole Polytechnique Federale de Lausanne, Switzerland (e-mail: andreas.burg@epfl.ch).

Mario Costanza is with Time & Frequency department, Femto-st research institute, Besançon, France (e-mail: mario.costanza@femto-st.fr)

Patrizia Livreri is with Department of Engineering, University of Palermo, Italy (e-mail: patrizia.livreri@unipa.it).

energy to power it, fewer components to assemble, and has smaller overall size for an energy autonomous wireless sensor node (EAWSN). The sensor architecture is also inherently digital, which compared to analog architectures, has a greater robustness to noise, does not require complicated electronics for the reading interface, as well as having a lower power consumption, which is a highly required feature, especially for energy autonomous and battery-free sensors [19]. The differentiating aspect of the present work with respect to comparable solutions [9], [20]–[22] is that our battery-free node is capable of sensing ambient light without using a dedicated light sensor and that all its components are decidedly off-the-shelf and readily available. The system performance characteristics and key features of the integrated circuits (ICs) used to power the node and transmit the data will be discussed in detail. The paper is organized as follows. Section II describes the system in terms of circuit implementation and functionality. Section III deals with the techniques and underlying logic used to measure light intensity from the magnitude of energy harvested by the EAWSN. Section IV deals with the design aspects of the EAWSN. Section V describes the system setup and environment and shows some experimental results. Section VI reports the final conclusions.

II. System Description

The system proposed in this paper and illustrated in Fig. 1 is energetically autonomous thanks to a photovoltaic transducer that simultaneously provides power and light sensing functionality, with a time domain readout communication protocol [23].

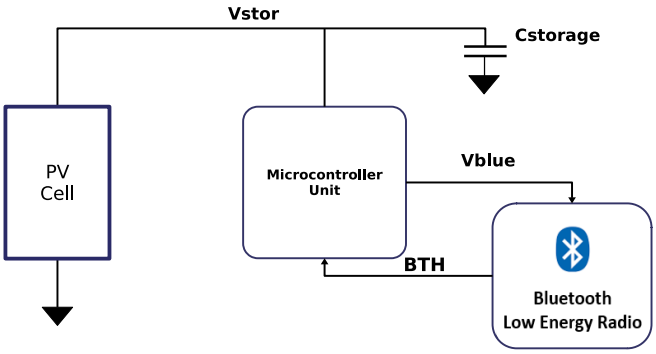

Fig. 1. System Block Diagram

Fig. 2 illustrates the operation of the system and shows how it alternates between an energy harvesting phase, in which ambient light energy is scavenged by the photovoltaic transducer and stored in the $C_{storage}$ capacitor, and a data transmission phase where the stored energy is used to supply the BLE radio. During the harvesting phase, the PV cell supplies a current that charges the capacitor $C_{storage}$ and causes a build-up of voltage V_{stor}. This voltage is monitored by the microcontroller unit (MCU), which operates in stop mode in this phase for ultra-low power consumption. When the voltage V_{stor} reaches the maximum value V_h, the system enters the data transmission phase, during which the MCU

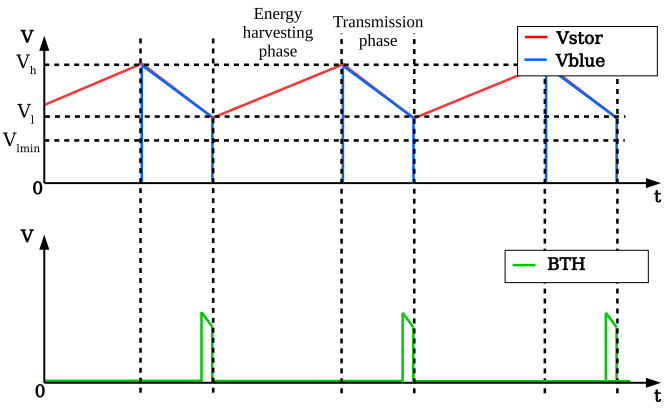

Fig. 2. Functional Description of the System

raises the voltage V_{blue} on one of its general purpose input/output (GPIO) pins that powers the BLE radio. During the transmission phase, the $C_{storage}$ capacitor must supply a current to the system that is in the order of milli-amperes, which is far in excess of the harvested current, which is on the order of tens of micro-amperes. This difference causes a drop in V_{stor}. As soon as the BLE radio has finished its radio activity, it raises the "BTH" (back to harvest) signal, which triggers the finite state machine (FSM) of the MCU to turn off the BLE radio by resetting the signal V_{blue}. This event causes the system to resume harvesting as described previously [24]. The main design challenge in an EAWSN is to manage the very limited amounts of energy. Hence, the ultra-low power STM32L0 microcontroller by STMicroelectronics [25] was selected as the best choice for the control and power management subsystem. Similar considerations are made when selecting the communication unit, which consumes most of the energy in the system. The BLE communication technology was therefore chosen for its low energy consumption, with appropriate link budget and its availability in smartphones. The Bluetooth low-energy SoC BLUENRG-2 provided by STMicroelectronics was selected [26].

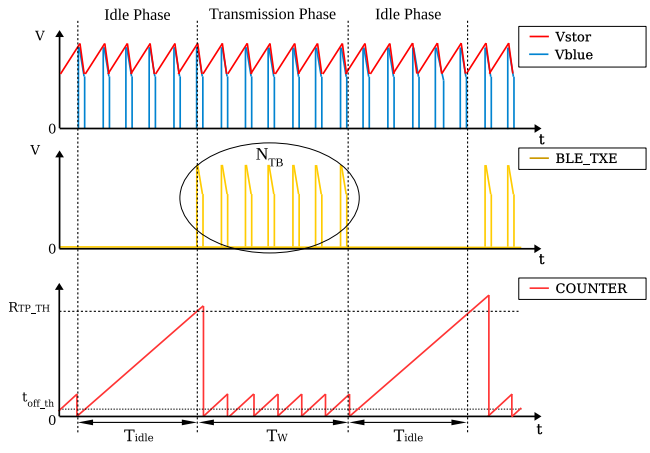

Fig. 3. Idle and transmission phases

To avoid flooding of the network with beacons which would impair other BLE devices operating in its range [27], [28], the number of broadcast events in a given time interval must be limited. For this, the EAWSN alternates between a transmission phase and an idle phase with the time interval (T_{idle}) as shown in Fig. 3. During the transmission phase the EAWSN broadcasts a number N_{TB} of beacons. During the idle phase, it is necessary to avoid that the voltage V_{stor} exceeds the maximum value V_h. Therefore, it is required to increase the current consumption of the system. To implement this feature, the BLE radio is enabled and configured only to receive bytes to use for the wireless configuration of the EAWSN, that is, to reconfigure the parameters T_{idle} and N_{TB}. In a typical use case, the transmission window time T_W is much lower than T_{idle}.

III. Light Intensity Measurement

A key aspect of the system described above is that the number of EAWSN transmissions to a remote base station (BS) in a given time interval varies proportionally with light intensity as shown in Fig. 4. We propose to specifically exploit this proportionality to realize an energy-proportional radio protocol that defers the intensity measurements to the BS which is powered by mains or a larger battery. To this end, we simply transmit N_{TB} BLE beacons during the transmission window time T_W. The BS, measures the time $t_{adv|i}$ with $i \in \{1, \cdots, (N_{RB}-1)\}$ between subsequent beacons, where N_{RB} is the effective number of received beacons by the BS.

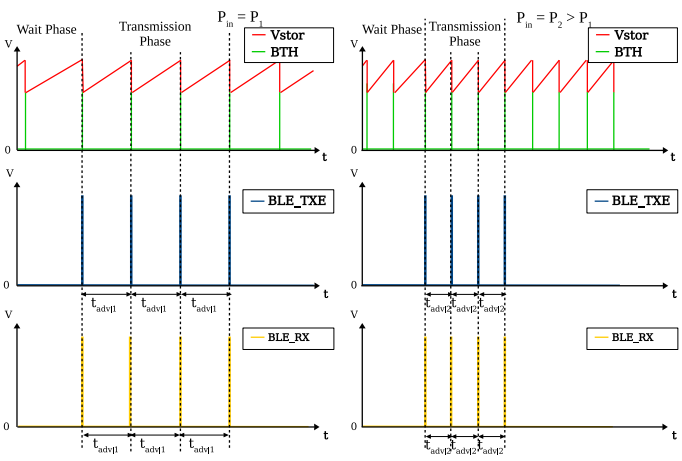

Fig. 4. Transmission phases with N_{TB} = 4 in two different light conditions (P_2, P_1). $P_2 > P_1$ implies that $t_{avg|2} < t_{avg|1}$

The BS is aware of both T_{idle} and N_{TB} parameters. Therefore, if $T_W \ll T_{idle}$, it can determine if the reception took place with the maximum expected number N_{TB} of beacons or if some beacons were lost. In fact, even if after the time T_{idle}, from the first received beacon, N_{RB} is lower than N_{TB}, the reception is considered concluded. The drawback of this solution is that lost beacons could lead to inaccurate illumination estimates. Nevertheless, under the hypothesis that $N_{RB} > \lceil N_{TB}/2 \rceil$, it is possible to avoid errors due to lost beacons in the beacon-based duty-cycle (light intensity) calculation in the BS, by considering the following two cases:

- Beacons are lost only within the transmission phase.
- Beacons are lost at one or both extremes of the transmission phase.

The identification of the relative position of a lost beacon within the transmission phase can be performed as follows:

- Calculate the minimum value of the time $t_{adv\_min\_BS}$ as:

$$t_{adv\_min\_BS} = min_{i \in \{1,\cdots,(NRB-1)\}} t_{adv|i} \quad (1)$$

- Compare each $t_{adv|i}$ with the threshold:

$$t_{adv\_th} = 1 + (\alpha) \cdot t_{adv\_min\_BS} \quad (2)$$

  with $\alpha \in [0, 1]$. In our implementation, we choose α = 0.2 also on the basis of experiments.
- If $t_{adv|i} > 1.2 \cdot t_{adv\_min\_BS}$ a beacon is considered lost within the transmission phase.
- Calculate the number of the beacons lost within the transmission phase, defined as N_{BLW}.
- Calculate the number of the beacons lost at the extremes of the transmission phase N_{BLE} as:

$$N_{BLE} = N_{TB} - N_{RB} - N_{BLW} \quad (3)$$

In the case of beacons lost only within the transmission phase, we observe that the transmission window time T_W measured at the EAWSN and BS are the same. Therefore, the time T_W can be expressed as:

$$T_W = (N_{TB} - 1) \cdot \overline{t_{adv}} \quad (4)$$

$$T_W = (N_{RB} - 1) \cdot \overline{t_{adv\_BS}} \quad (5)$$

where:

- $\overline{t_{adv}}$ is the average value of the set of values $t_{adv|i}$ with $i \in \{1, \cdots, (N_{TB} - 1)\}$.
- $\overline{t_{adv\_BS}}$ is the average value of the set of values $t_{adv|i}$ with $i \in \{1, \cdots, (N_{RB} - 1)\}$, measured at the BS.

from Eq. (4) and (5), it is possible to derive the $\overline{t_{adv}}$ from the time $\overline{t_{adv\_BS}}$ measured by the BS as:

$$\overline{t_{adv}} = \frac{\overline{t_{adv\_BS}} \cdot (N_{RB} - 1)}{N_{TB} - 1} \quad (6)$$

In the case of beacons lost at one or both extremes of the transmission phase, we observe that the transmission window time reduced by the beacons at the extremes T_{WR} can be expressed as:

$$T_{WR} = (N_{TB} - N_{BLE} - 1) \cdot \overline{t_{adv}} \quad (7)$$

$$T_{WR} = (N_{RB} - 1) \cdot \overline{t_{adv\_BS}} \quad (8)$$

from Eq. (7) and (8), it is possible to derive the $\overline{t_{adv}}$ from the time $\overline{t_{adv\_BS}}$ actually measured at the BS as:

$$\overline{t_{adv}} = \frac{\overline{t_{adv\_BS}} \cdot (N_{RB} - 1)}{N_{TB} - N_{BLE} - 1} \tag{9}$$

Since the BS has both the N_{RB} and N_{TB} parameters, it is possible to evaluate the quality of communication (QoC) between the BS and the EAWSN. To do this, the QoC parameter, defined as a percentage ratio between the number N_{RB} of beacons received and the number N_{TB} of expected beacons, can be calculated using (10).

$$QoC = 100 \cdot \frac{N_{RB}}{N_{TB}} \tag{10}$$

It must be considered that the described method is valid if it is respected the following condition:

$$t_{adv\_min\_BS} = t_{adv\_min} \tag{11}$$

Where t_{adv_min} is the minimum advertising time of the beacons emitted by the EAWSN. This mathematical result can be conveniently converted into the practical condition, easily implemented in the BS firmware, that only if $N_{RB} > \lceil N_{TB}/2 \rceil$ the BS can consider the calculated data tenable. Therefore, the validity of this method is based on the assumption that communication quality is sufficiently high as it happens in a typical application case. The BS can therefore receive beacons from one or more EAWSNs and exercise control functions of the ambient brightness by automatically controlling, for example, dimmable lamps, rolling shutters, awnings, etc. Therefore, the BS can be easily configured and updated periodically by the user, e.g. to calibrate and compensate for the degradation of photovoltaic performance over time or to set different lighting thresholds that allow customized home automation control.

IV. EAWSN System Design and Light Calibration Requirement

The experimental measurements shown in Fig. 5 reveal how the EAWSN can be exposed to a wide range of ambient light conditions, which can vary by more than two orders of magnitude from a minimum of 200 lux to values that can exceed 50000 lux.

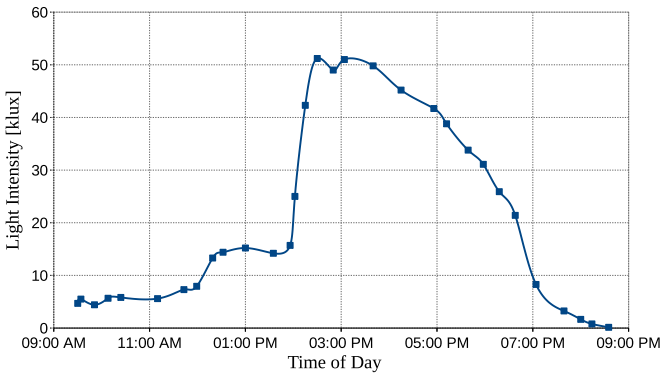

Fig. 5. Light intensity vs daytime (data acquired in June 2020, Lat:37°18'26.8", Lon:13°35'37.4" with the EAWSN facing South)

For low light intensity, the design challenge is to ensure that the system can operate down to the lowest possible limit of detection (LoD). For high intensity light the number of broadcast events in a given time interval must be limited. Another issue involving very high light intensity, i.e., when the sensor saturates, is that the advertising interval t_{adv} can fall below 100 ms, which is no longer compatible with the Bluetooth standard specification [29]. Fig. 6 shows experimental measurements where t_{adv} does indeed fall below 100 ms when the light intensity is higher than 17000 lux and there is no intervention to limit t_{adv}. Fig. 7 provides a graphical representation of how t_{adv} is linked to the system parameters t_{rise}, t_{fall}, V_h and V_l for given values of the capacitor $C_{storage}$, light intensity E_v, and the power conversion efficiency (PCE) of the photovoltaic transducer. The system parameter t_{rise} is the charging time of the capacitor $C_{storage}$ from the minimum value V_l to the maxim value V_h of the voltage V_{stor}. The system parameter t_{fall} is the discharging time of the capacitor $C_{storage}$ from the maximum value V_h to the minimum value V_l of the voltage V_{stor}. Equation (12) shows how t_{adv} is related to the charging time t_{rise} and the discharging time t_{fall}. Therefore, any control of t_{adv} can be indirectly performed by acting on one or both the parameters t_{rise} and t_{fall}.

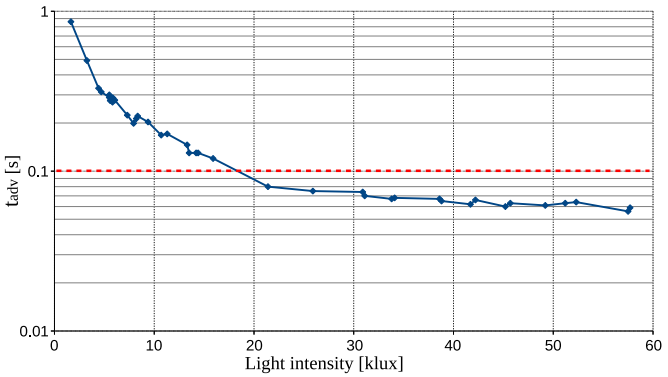

Fig. 6. t_{adv} vs light intensity without data rate control

$$t_{adv} = t_{rise} + t_{fall} \tag{12}$$

Equation (13) shows how the value of the time t_{fall} is linked to the value of the total system power consumption P_{tot}, the system parameters V_h and V_l and component parameter $C_{storage}$.

$$t_{fall} = \frac{C_{storage} \cdot (V_h^2 - V_l^2)}{2 \cdot P_{tot}} \tag{13}$$

Equation (14) shows how the value of the time t_{rise} is linked to received input power P_{in}, the quiescent power consumption P_q, the PCE of the photovoltaic transducer, the system parameters V_h and V_l and the component parameter $C_{storage}$,

$$t_{rise} = \frac{C_{storage} \cdot (V_h^2 - V_l^2)}{2 \cdot (PCE \cdot P_{in} - P_q)} \tag{14}$$

These equations suggest that control of t_{adv} can be optimized for a wide input power P_{in} range in various ways, each with its advantages and disadvantages. The method discussed in this paper implements full digital control of the

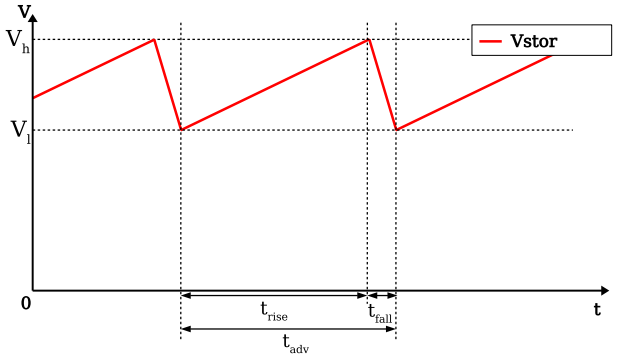

Fig. 7. System parameters t_{rise}, t_{fall}, V_h and V_l on t_{adv}

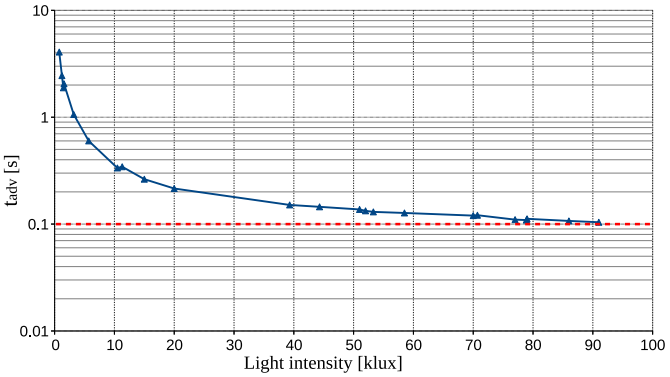

Fig. 9. t_{adv} vs light intensity with t_{fall_th} set to 70 ms

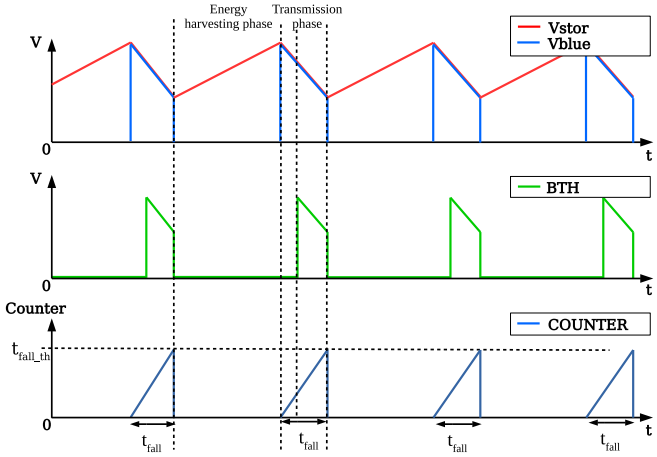

Fig. 8. System's signals for the control of the time t_{fall}

advertising interval by only varying the time t_{fall}, since t_{rise} cannot increase independently of V_h and $C_{storage}$. The voltage threshold V_h cannot increase any further as it is already close to the maximum voltage tolerated by the ICs. Further, it is usually preferable to keep $C_{storage}$ to a minimum, especially in applications with stringent miniaturization specifications. Since the BLE radio is only turned on during transmission, control of t_{adv} must be performed by the MCU, which is always on, even in the ultra-low power stop mode. This solution uses the 16-bit LPTIM timer of the STM32L0 IC, which is driven by a 31 kHz clock that adds a negligible overhead of only 10 nA to the overall system quiescent current consumption I_q of $\approx 1\ \mu A$. Fig. 8 shows how the LPTIM timer allows the system to switch from the transmission to energy harvesting phase when the timer LPTIM crosses the threshold t_{fall_th} (e.g. 100 ms). The LPTIM timer is started by software at the beginning of every data transmission phase. Fig. 9 shows an example with t_{fall_th} = 70 ms, for which the advertising duty cycle of the device remains compatible with the BLE standard up to $\approx$ 100 klux.

Another design consideration of the EAWSN is maximizing the scavenged energy conversion efficiency, which is heavily dependent on the choice of the photovoltaic transducer. Since the photovoltaic cell is also used for light sensing, the LoD is another important parameter in terms of light intensity performance. For these reasons, as well as the size and weight requirements, the PCE and maximum power point (MPP) at the minimum specified light intensity of 200 lux are critical factors. The MPP of a photovoltaic energy source is the operating condition where the power transfer from the source to the load is maximized. This condition, as illustrated in Fig. 10, is represented by the coordinates (V_{MPPT} and I_{MPPT}), which represent the maximum power point voltage and the maximum power point current, respectively.

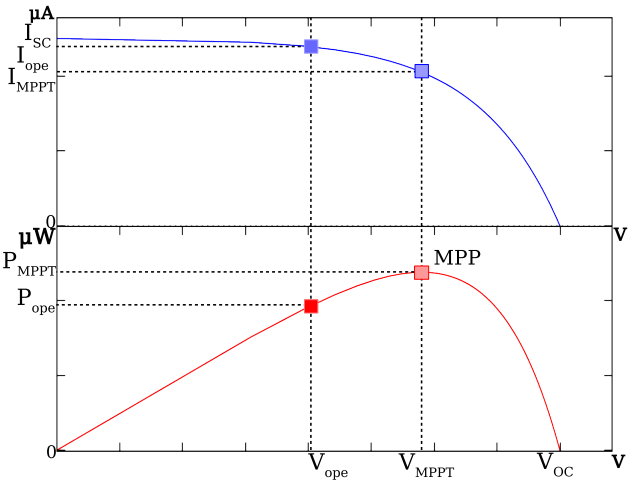

Fig. 10. Electrical Properties of the Photovoltaic Cell

To attenuate the high sensitivity of the system to the current at the MPP working point, the operating point of the voltage V_{stor} is selected as the recommended voltage V_{ope}, which is close to and sufficiently lower than the voltage V_{MPPT}. In addition to these considerations, the value of the voltage V_{ope} must lie within the supply operating voltage range [1.8 – 3.6] V of the STM32L0 and BLUENRG-2 ICs. While the system is harvesting energy, the BLE radio is off and the system load consists only of the MCU. During the scavenging phase, only the internal power voltage detector (PVD) and the CPU are active in the MCU. According to the STM32L0 data-sheet [25], the typical total current consumption I_{mcu} and the total quiescent current I_q of the system during the energy harvesting phase is therefore $\approx 1\ \mu A$, which is in fact the minimum current necessary for the system to operate, and which ultimately defines the LoD of the system. For this type

of application, reducing I_q as much as possible is essential to obtain lower values of LoD and, therefore, to be able to make a smaller implementation or operate in even dimmer lighting conditions. While the system is harvesting energy, the $C_{storage}$ capacitor is charged by the current provided by the harvester. However, a positive difference between the current supplied by the photovoltaic source and the current delivered to the load is required, especially at the specified minimum light intensity of 200 lux. For this reason, the photovoltaic harvester must provide a current higher than the minimum current of 1 μA. This requirement is met by the amorphous silicon solar cell AM-1606C by Panasonic [30], which provides a typical output current I_{ope} of 3.4 μA at the voltage V_{ope} of 2.6 V for a light intensity of 200 lux, and its maximum overall dimensions are 15 x 15 x 0.9 mm. The energy consumption of the system during the transmission phase equates to the sum of the MCU and BLE radio consumption. The BLE radio of the battery-free device is programmed to operate in non-connectable advertising mode, to transmit an output power of 8 dBm over three different channels, with 7-byte advertising data packets. In these conditions, the BLUENRG-2 IC has a total average current consumption of ≈ 7 mA during the active phase, when biased with a voltage of 2.6 V, and completes the data transmission in ≈ 2 ms, which results in an energy consumption E_{BLE_TX} of ≈ 37 μJ. The MCU during the RUN mode and under typical working conditions, with clock frequency 1 MHz and internal bias regulated voltage of 1.8 V, has a current consumption of ≈ 2 mA and an average value of ≈ 90 μA, which corresponds to an energy consumption of ≈ 9.5 μJ per work cycle. Hence, even in RUN mode, the power consumption of the MCU IC is almost four times lower than that of the BLE radio IC. In these working conditions, the total energy consumption of the system can therefore be approximated as $E_{tot} \approx 50\,\mu J$. Table I reveals a summary of the power performance for each component used in the system.

Component	Operating Condition	Power
STM32L01F4	Stop Mode $V_{stor\_avg} = 2.6\,V$	2.6 μW
STM32L01F4	Run Mode $V_{stor\_avg} = 2.6\,V$	3.6 mW
Bluenrg-M2SP	Advertising Mode Non-connectable undirected event P_{out} = 8 dBm Data Length = 7 bytes $V_{stor\_avg} = 2.6\,V$	18.5 mW
AM-1606C	200 lux Temperature = 25 °C $V_{stor\_avg} = 2.6\,V$	8.84 μW

TABLE I
EAWSN COMPONENTS POWER SUMMARY

The maximum value V_h of the voltage V_{stor} is chosen as 3.3 V to comply with the maximum supply voltage of both the STM32L0 and the BLUENRG-2 IC. The average value of the voltage V_{stor} is given by:

$$V_{stor\_avg} = \frac{V_h + V_l}{2} \tag{15}$$

In order to obtain optimum power conversion performance from the photovoltaic transducer, the average value of the voltage V_{stor_avg} is chosen equal to the voltage V_{ope}. From this, the minimum value V_l of the voltage V_{stor} is calculated according to:

$$V_l = 2 \cdot V_{ope} - V_h = 1.9\,V \tag{16}$$

It follows that the value of the $C_{storage}$ capacitor can be calculated as:

$$C_{storage} \geq \frac{2 \cdot E_{tot}}{V_h^2 - V_l^2} = 14\,\mu F \tag{17}$$

In order to integrate a certain degree of margin and thereby render the system performance less sensitive to the inevitable parametric variations of the various components involved, the capacitor chosen for this application is a 22 μF capacitor. The chosen values of the voltages V_h and V_l and that of the $C_{storage}$ capacitor allow for:

$$E_{harvested} = \frac{C_{storage} \cdot (V_h^2 - V_l^2)}{2} = 80\,\mu J \tag{18}$$

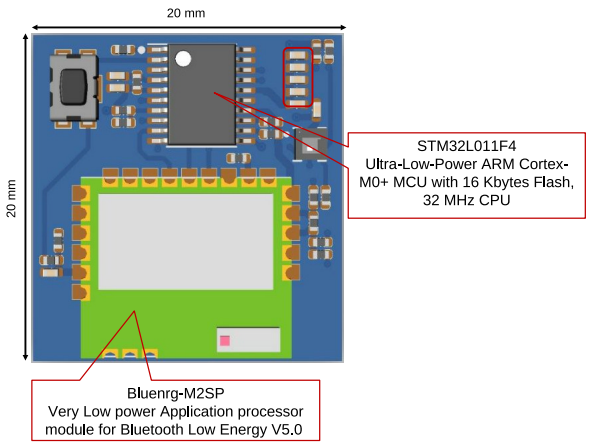

Fig. 11. EAWSN PCB top view

V. Experimental Results

Fig. 11 shows the top view of the PCB that was used to obtain experimental data. The top view shows the commercially available, off-the-shelf devices used to create the system. For BLE radio communication, the BLUENRG-M2SP very low power application processor module for Bluetooth® low energy v5.0 [26] is used. The ultra-low power operation and high system efficiency are obtained through careful hardware and software co-design of the STM32L0 MCU, which also manages the sensor. Fig. 12 shows the system in a typical home environment. The BS was implemented with the BLUENRG-2 IC set to scanning mode to receive the data transmitted by the battery-free EAWSN, configured in advertising non-connectable mode to transmit an output power of 8 dBm. The BLE EAWSN and the BS were placed at an average distance of 5 meters. During the measurements, several other devices using Bluetooth and Wi-Fi were active, including a 2.4 GHz Wi-Fi access-point and various personal computers and smart-devices. Numerous tests under these conditions were conducted in order to expose the EAWSN to various

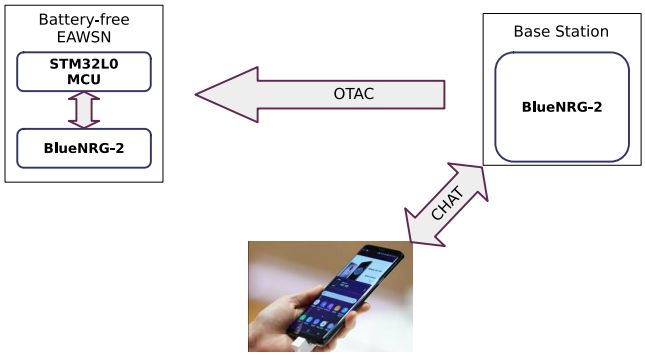

Fig. 12. Battery-free EAWSN and BS system

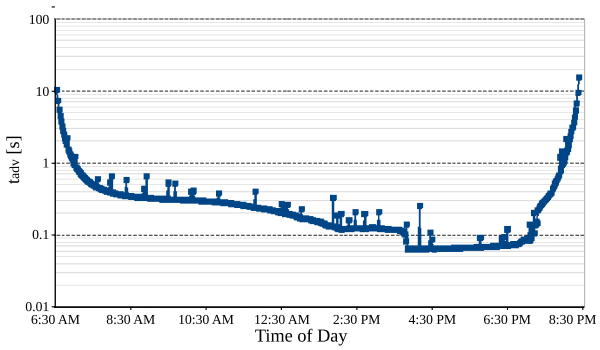

Fig. 13. t_{adv} vs daytime (log scale)
Data acquired in July 2020
Latitude: 37°18'26.8", Longitude: 13°35'37.4"

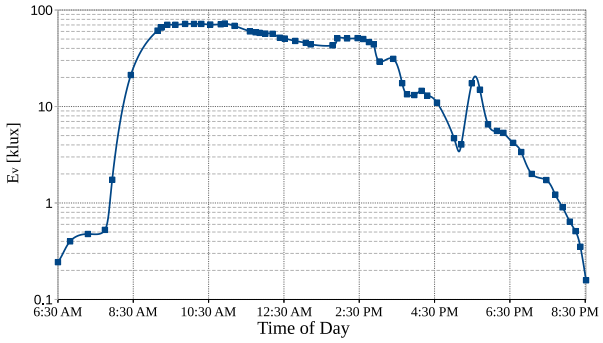

Fig. 14. Light intensity vs daytime
Data acquired in July 2020
Latitude: 37°18'26.8", Longitude: 13°35'37.4"

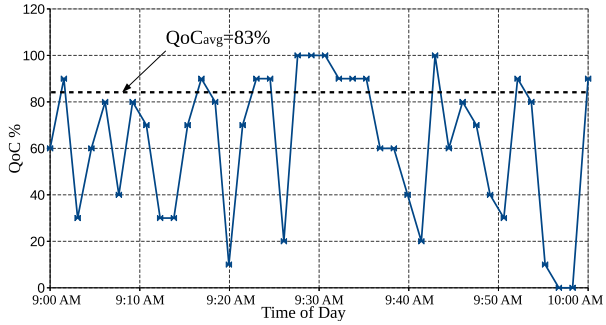

Fig. 15. Quality of the communication (QoC) in the time frame 9:00 AM-10:00 AM

ambient light intensities. The most relevant signals, such as the V_{stor} voltage, the V_{blue} voltage on the battery-free BLE sensor, and the received "BLE_RX" data signal on the BS, were observed, monitored, and measured. The data rate of the wireless data transfer operation was controlled as described in Section IV, and both the EAWSN and the BS were configured to work with an T_{idle} of 60 sec and N_{TB} = 10. The data received by the BS were monitored and recorded over the course of an entire day. Time was recorded t_{adv_avg} and reference ambient light intensity measurements were performed by using the luxmeter (PCE-174 and UNI-T UT382). Fig. 13 and Fig. 14 show the variations of the time t_{adv_avg} and the light intensity versus the daytime, respectively. These measurements were performed during a series of tests conducted between April and July 2020. Fig. 15 shows a sample of the measured QoC values over an hour. Fig. 16 shows the relationship between the time t_{adv} measured by the BS and the measurement of the light intensity carried out by means of the luxmeter during various hours of the day. Fig. 17 shows the characterization results, performed over ten different measurements, of $1/t_{adv}$ versus the illuminance E_v in the range $[225, 90000]$ lux. We observe that, according to our expectations, the curve has a monotonous trend allowing a linear approximation. The solid line curve shows the measured values, the dotted line reveals the boundaries due to the maximum measurement uncertainty of $10 \cdot 10^{-2}$ Hz.

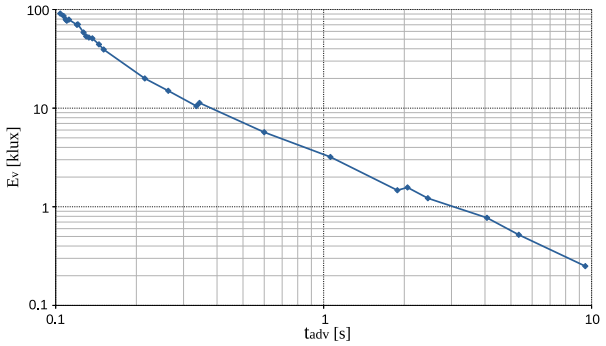

Fig. 16. Light intensity vs t_{adv}

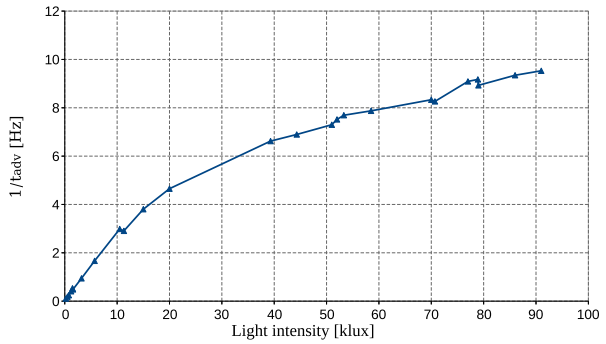

Fig. 17. $1/t_{adv}$ vs light intensity

VI. Conclusions

In this paper, an Energy Autonomous Wireless Sensor Node (EAWSN) with BLE communication for ambient light sensing has been proposed, designed, and experimentally tested. It was shown that the system, consisting of the EAWSN and the Base Station (BS), is capable of performing ambient light power measurements without the use of batteries or external power sources. It was highlighted how the notion that the physical quantity being sensed, and the source of energy are one and the same, allowing major simplification of the EAWSN architecture. An important aspect of this study is that the same underlying concept can be extended to other sources of ambient energy, such as kinetic, thermal, and so on. It was shown how the simplicity of the architecture translates into an effective advantage in terms of size, energy and cost, and how it is possible to configure a set-and-forget device in virtually any environment where light is available. Finally, the experimental results from measurements performed on a 2 cm x 2 cm tag size PCB, implemented with off-the-shelf components have been provided to demonstrate the viability of the system and operational performance.

References

[1] T. W. Foster, D. V. Bhatt, G. P. Hancke, and B. Silva, "A web-based office climate control system using wireless sensors," *IEEE Sensors Journal*, vol. 16, no. 15, pp. 6104–6113, 2016.

[2] S. D. T. Kelly, N. K. Suryadevara, and S. C. Mukhopadhyay, "Towards the implementation of iot for environmental condition monitoring in homes," *IEEE sensors journal*, vol. 13, no. 10, pp. 3846–3853, 2013.

[3] W. Dargie, "Dynamic power management in wireless sensor networks: State-of-the-art," *IEEE Sensors Journal*, vol. 12, no. 5, pp. 1518–1528, 2012.

[4] M. Zhu, M. Hassanalieragh, Z. Chen, A. Fahad, K. Shen, and T. Soyata, "Energy-aware sensing in data-intensive field systems using supercapacitor energy buffer," *IEEE Sensors Journal*, 2018.

[5] M. Alioto and M. Shahghasemi, "The internet of things on its edge: Trends toward its tipping point," *IEEE Consumer Electronics Magazine*, vol. 7, no. 1, pp. 77–87, 2018.

[6] B. Martinez, M. Monton, I. Vilajosana, and J. D. Prades, "The power of models: Modeling power consumption for iot devices," *IEEE Sensors Journal*, vol. 15, no. 10, pp. 5777–5789, 2015.

[7] T. Soyata, L. Copeland, and W. Heinzelman, "RF energy harvesting for embedded systems: A survey of tradeoffs and methodology," *IEEE Circuits and Systems Magazine*, vol. 16, no. 1, pp. 22–57, 2016.

[8] C. Trigona, B. Andò, S. Baglio, R. La Rosa, and G. Zoppi, "Sensors for kinetic energy measurement operating on "zero-current standby"," *IEEE Transactions on Instrumentation and Measurement*, vol. 66, no. 4, pp. 812–820, 2017.

[9] C. Abella, S. Bonina, A. Cucuccio, S. D'Angelo, G. Giustolisi, A. Grasso, A. Imbruglia, G. Mauro, G. Nastasi, G. Palumbo *et al.*, "Autonomous energy-efficient wireless sensor network platform for home/office automation," *IEEE Sensors Journal*, 2019.

[10] S. Senivasan, M. Drieberg, B. S. M. Singh, P. Sebastian, and L. H. Hiung, "An mppt micro solar energy harvester for wireless sensor networks," in *2017 IEEE 13th International Colloquium on Signal Processing & its Applications (CSPA)*. IEEE, 2017, pp. 159–163.

[11] S. Y. Heo, J. Kim, P. Gutruf, A. Banks, P. Wei, R. Pielak, G. Balooch, Y. Shi, H. Araki, D. Rollo *et al.*, "Wireless, battery-free, flexible, miniaturized dosimeters monitor exposure to solar radiation and to light for phototherapy," *Science translational medicine*, vol. 10, no. 470, p. eaau1643, 2018.

[12] R. La Rosa, C. Dehollain, and P. Livreri, "Advanced monitoring systems based on battery-less asset tracking modules energized through rf wireless power transfer," *Sensors*, vol. 20, no. 11, p. 3020, 2020.

[13] R. La Rosa, P. Livreri, C. Trigona, L. Di Donato, and G. Sorbello, "Strategies and techniques for powering wireless sensor nodes through energy harvesting and wireless power transfer," *Sensors*, vol. 19, no. 12, p. 2660, 2019.

[14] R. La Rosa, C. Dehollain, F. Pellitteri, R. Miceli, and P. Livreri, "An rf wireless power transfer system to power battery-free devices for asset tracking," in *2019 26th IEEE International Conference on Electronics, Circuits and Systems (ICECS)*. IEEE, 2019, pp. 534–537.

[15] R. La Rosa, G. Zoppi, L. Di Donato, G. Sorbello, A. Di Carlo, and P. Livreri, "A battery-free smart sensor powered with rf energy," in *4th International Forum on Research and Technology for Society and Industry (RTSI)*. IEEE, 2018, pp. 1–4.

[16] G. Loubet, A. Takacs, and D. Dragomirescu, "Implementation of a battery-free wireless sensor for cyber-physical systems dedicated to structural health monitoring applications," *IEEE access*, vol. 7, pp. 24 679–24 690, 2019.

[17] R. La Rosa and C. Trigona, "A fully autonomous platform for power measurement of environmental rf sources based on a time domain readout," *Measurement*, p. 108115, 2020.

[18] R. La Rosa, "Sensor, corresponding system and operating method," September 2020. [Online]. Available: https://www.freepatentsonline.com/y2020/0303952.html

[19] S. Middelhoek, P. French, J. Huijsing, and W. Lian, "Sensors with digital or frequency output," *Sensors and actuators*, vol. 15, no. 2, pp. 119–133, 1988.

[20] S. N. R. Kantareddy, I. Mathews, S. Sun, M. Layurova, J. Thapa, J.-P. Correa-Baena, R. Bhattacharyya, T. Buonassisi, S. E. Sarma, and I. M. Peters, "Perovskite pv-powered rfid: enabling low-cost self-powered iot sensors," *IEEE Sensors Journal*, vol. 20, no. 1, pp. 471–478, 2019.

[21] L. Joris, F. Dupont, P. Laurent, P. Bellier, S. Stoukatch, and J.-M. Redouté, "An autonomous sigfox wireless sensor node for environmental monitoring," *IEEE Sensors Letters*, vol. 3, no. 7, pp. 01–04, 2019.

[22] J. S. Y. Tan, J. Park, J. Li, Y. Dong, K. H. Chan, G. W. Ho, and J. Yoo, "A 0.14 pj/conversion fully energy-autonomous temperature-to-time converter for biomedical applications," *IEEE Solid-State Circuits Letters*, 2020.

[23] B. Andò, S. Baglio, and A. Beninato, "A ferrofluid inclinometer with a time domain readout strategy," *Sensors and Actuators A: Physical*, vol. 202, pp. 57–63, 2013.

[24] R. Larosa and G. Zoppi, "Method of operating radio-frequency powered devices, corresponding circuit and device," 2018, uS Patent App. 15/975,347.

[25] STMicroelectronics, "Ultra-Low-Power 32-bit MCU Arm-Based Cortex-M0+, up to 64 KB Flash Memory, 8 KB SRAM, 2 KB EEPROM, USB, ADC, DAC, STM32L052x6 STM32L052x8 datasheet," in *Available online: https://www.st.com (accessed on June 20th, 2020)*. STMicroelectronics Geneva,Switzerland, 2014.

[26] ——, "Bluerng-M2SP very low power application processor module for bluetooth® low energy v5.0," in *Available online: https://www.st.com/resource/en/datasheet/bluenrg-m2.pdf (accessed on June 20th, 2020)*. STMicroelectronics Geneva,Switzerland, 2010.

[27] T.-Y. Lin, Y.-K. Liu, and Y.-C. Tseng, "An improved packet collision analysis for multi-bluetooth piconets considering frequency-hopping guard time effect," *IEEE Journal on Selected Areas in Communications*, vol. 22, no. 10, pp. 2087–2094, 2004.

[28] S. Y. Shin, H. S. Park, S. Choi, and W. H. Kwon, "Packet error rate analysis of zigbee under wlan and bluetooth interferences," *IEEE Trans. on Wireless Communications*, vol. 6, no. 8, pp. 2825–2830, 2007.

[29] C. S. W. Group, *Bluetooth Core Specification*, v5.2 ed., Bluetooth Special Interest Group (SIG), core-main@bluetooth.org, Dec. 2019. [Online]. Available: https://www.bluetooth.com/specifications/bluetooth-core-specification/

[30] *Amorton Solar Cell Catalog*, Panasonic, Jul. 2019. [Online]. Available: https://www.panasonic-electric-works.com/eu/amorton-amorphous-silicon-solar-cells.htm

Roberto La Rosa (M'20) received the Master's degree (cum laude) in electronics engineering from the University of Palermo, Italy, in 1995. Currently, he is a Ph.D. student in Electrical Engineering at the Ecole Polytechnique Federale de Lausanne (EPFL), Switzerland. Since 1997 he has been a senior analog and mixed-signal IC designer with STMicroelectronics, where he is currently Senior Member of the Technical Staff, IC Design Manager, and ultra-low-power application team manager. His current research interests include ultra-low-power applications, Wireless Power Transfer, and Energy Harvesting. He has published several scientific papers on advanced techniques for Energy Harvesting and Wireless Power Transfer and holds several patents.

Catherine Dehollain received the Master's degree in electrical engineering and the Ph.D. degree from Ecole Polytechnique Federale de Lausanne (EPFL), Lausanne, Switzerland, in 1982 and 1995, respectively. From 1982 to 1984, she was a Research Assistant at the Electronics Laboratories (LEG), EPFL. In 1984, she joined the Motorola European Center for Research and Development, Geneva, Switzerland, where she designed integrated circuits applied to telecommunications. In 1990, she joined EPFL as a Senior Assistant at the Chaire des Circuits et Systemes, where she was involved in impedance broadband matching. Since 1995, she has been responsible for the RFIC Group, EPFL, for RF activities. She has been the Technical Project Manager of the European projects, Swiss CTI projects, and the Swiss National Science Foundation projects dedicated to RF wireless micro-power sensor networks and mobile phones. Since 1998, she has been a Lecturer at EPFL in the area of RF circuits, electric filters, and low power CMOS analog circuits. From 2006 to 2014, she was a Maitre d'Enseignement et de Recherche (MER) at EPFL. Since 2014, she has been Adjunct Professor at EPFL. She is an author or coauthor of seven scientific books and of 190 scientific publications. Her current research interests include biomedical remotely powered sensors, RFIDs, RF circuits, low power analog circuits, and electrical filters.

Andreas Burg (S'97-M'05) was born in Munich, Germany, in 1975. He received his Dipl.-Ing. degree from the Swiss Federal Institute of Technology (ETH) Zurich, Zurich, Switzerland, in 2000, and the Dr. sc. techn. degree from the Integrated Systems Laboratory of ETH Zurich, in 2006. In 1998, he worked at Siemens Semiconductors, San Jose, CA. During his doctoral studies, he worked at Bell Labs Wireless Research for a total of one year. From 2006 to 2007, he was a postdoctoral researcher at the Integrated Systems Laboratory and at the Communication Theory Group of the ETH Zurich. In 2007 he co-founded Celestrius, an ETH-spinoff in the field of MIMO wireless communication, where he was responsible for the ASIC development as Director for VLSI. In January 2009, he joined ETH Zurich as SNF Assistant Professor and as head of the Signal Processing Circuits and Systems group at the Integrated Systems Laboratory. In January 2011, he joined the Ecole Polytechnique Federale de Lausanne (EPFL) where he is leading the Telecommunications Circuits Laboratory. He was promoted to Associate Professor with Tenure in June 2018. Mr. Burg has served on the TPC of various conferences on signal processing, communications, and VLSI. He was a TPC co-chair for VLSI-SoC 2012 and the TCP co-chair for ESSCIRC 2016 and SiPS 2017. He was a General Chair of ISLPED 2019 and he served as an Editor for the IEEE Transaction of Circuits and Systems in 2013 and on the Editorial board of the Springer Microelectronics Journal. He is currently an editor of the Springer Journal on Signal Processing Systems, the MDPI Journal on Low Power Electronics and its Applications, and of the IEEE Transactions on VLSI. He is also a member of the EURASIP SAT SPCN and the IEEE CAS-VSATC.

Mario Costanza received the Master's degree (cum laude) in electronics engineering from the University of Palermo, Italy, in 2020. Currently, he is a PhD student at the Femto-ST Institute of Besançon, France. His research interests include Energy Harvesting, Energy-Autonomous Wireless sensors, piezoelectric materials, graphene and Surface Acoustic Wave (SAW) devices.

Patrizia Livreri (M'94) received the Master's degree (cum laude) in electronics engineering and the Ph.D. degree from the University of Palermo (UNIPA), Italy, in 1986 and 1992, respectively. From 1987 to 1989, she was with Elettronica SpA (Leonardo company), Roma, Italy, where she designed microwave integrated circuits. In 1993, she joined the National Research Center CNR as a Researcher where she was involved in microwave low noise amplifier design. Since 1994, she has been an Adjunct Professor at UNIPA where she serves as a director of the Power Electronics Laboratory. She is an author or co-author of scientific books and of 160 scientific publications. Her current research interests include energy harvesting, wireless power transfer, remotely powered sensors.